Chemical Engineering Journal 466 (2023) 143003

Contents lists available at ScienceDirect

Chemical Engineering Journal

journal homepage: www.elsevier.com/locate/cej

Unprecedented facile approach of multiple amino-substituted triphenylamine derivatives for electrochromic devices with extremely high coloration efficiency and unexpected redox stability

Yu-Jen Shao [1], Min-Hsiu Tu [1], Guey-Sheng Liou

Institute of Polymer Science and Engineering, National Taiwan University, No. 1, Sec. 4, Roosevelt Rd., Taipei 10617, Taiwan

ARTICLE INFO

Keywords:
Triphenylamine derivatives
Electrochromism
High stability
Amino substituent
High coloration efficiency

ABSTRACT

Generally, the amino group is considered highly reactive and unstable. Thus, the amino derivatives would be entirely consumed by polymerization or end-capping to preserve the material stability in most research or application fields. Herein, we demonstrated that triphenylamine (**TPA**) with multiple *para*-amino substituents could reduce oxidation potential and provide extra oxidation sites while retaining their reversibility. Four *para*-amino-substituted **TPA** derivatives (**TPA-1N**, **TPA-2N**, **TPA-3N**, and **TPA-ADM**) designed and prepared in this study exhibited excellent stability under the electrochemical redox procedure, revealing more than 88% reversibility in the continuous cyclic voltammetry process up to 10,000 cycles. Among all the electrochromic devices, **TPA-3N/HV** performs the highest coloration efficiency (631 cm^2/C), coloration speed (46.4 % s^{-1}), and superior stability, manifesting a reversibility of 99% or 98% after 1000 cycles (switching) or 10 h (maintaining at coloring state), respectively.

1. Introduction

The electrochromic (EC) materials present a reversible change in the optical properties under an applied voltage [1]. In general, the transition of the colors includes the bleached and the colored states and is utilized in smart windows, anti-glare glass, and transparent displays nowadays [2–5]. To optimize the EC devices (ECDs), the EC materials must possess fast response speed, high contrast ratio, low driving voltage, and long-term stability [6–9]. Coordination metal complexes, consisting of transition metal ions and small molecular ligands, and transition metal oxides are two common approaches for preparing EC materials. The combination of different metal ions and ligands can generate a range of colors during the redox process controlled by the gap of MLCT [10–14]. Besides, metal oxides such as WO_3 and NiO also have been widely used and further developed for multi-metal oxide-containing materials to study their electrochromic behaviors [15,16]. Meanwhile, the small organic molecules are also attractive to the researchers owing to their nature, ease of preparation, lower oxidation potentials, higher neutral state transmittance, and shorter response time [17–19]. Viologen is a typical cathodic EC material for small organic molecules [20–22]. After the reduction from the colorless dication, the cation radical exhibits intense color due to the intrinsic intramolecular charge transfer [23].

TPA derivatives have been considered one of the appropriate EC materials with high performance and superior electrochemical stability [24]. After an electron is removed from the lone pair of the nitrogen center in the **TPA** molecule, the propeller-shaped structure flattens and transforms to higher conjugated conformation with the characteristic absorption peaks generated at the visible light region [25]. Modified by different substituents or functional moieties, the optoelectronic properties of the **TPA** derivatives would be tunable and diversified [26,27]. Several methods have been reported to enhance the EC properties of the **TPA** derivatives. Electron-donating groups (EDGs), such as methoxy and methyl groups, are commonly decorated to the *para*-position of the **TPA** molecule [17,18,28–30]. The electron-donating ability of these EDGs could effectively reduce the oxidation potential, and the *para*-orientated substituents prevent the dimerization of the **TPA** derivatives, resulting in enhanced redox stability. A mixed-valence chromophore could lower not only the first oxidation potential of the molecules but also enrich the EC behaviors of more oxidation states. Consequently, by adding electroactive substituents such as dimethylamino, diphenylamino, and triphenylamine moieties, the conjugated connection between the **TPA** unit and the additional redox-active sites results in the mixed-valence system [17,26]. Moreover, a photoexcited electron transfer happens from the extra neutral nitrogen center to the **TPA** radical cation center, resulting

E-mail address: gsliou@ntu.edu.tw (G.-S. Liou).
[1] The authors contributed equally.

https://doi.org/10.1016/j.cej.2023.143003
Received 16 January 2023; Received in revised form 11 April 2023; Accepted 13 April 2023
Available online 23 April 2023

in the intervalence charge-transfer (IV-CT) absorption band at the NIR region [31,32]. Other than the substituent mentioned above, the amino substituent is an influential electron-donating group that inclines to oxidize under externally applied potential. Thus, the unprotected amino substituents are considered unstable and deteriorate quickly. Consequently, the amino-substituted EC materials would be prepared as polymers or other functionalized small molecular derivatives to preserve durability in most studies [33–36]. Nevertheless, after the procedures of the amidization or imidization to obtain polyamides or polyimides, the amino groups lose the original capability of further oxidation, sacrificing the electrochemical behavior of the additional oxidation sites.

A couple of amino-substituted **TPA** derivatives as the monomers used to prepare the corresponding electroactive polymers in previous studies [37–39]. However, these monomers would be potentially remarkable EC materials with lower oxidation potential and extra redox-active sites from the amino groups. Moreover, the preparation of the ECDs could be simplified without the polymerization procedure. In 2005, our group investigated the electrochemical properties of a series of *para*-amino-substituted **TPA** derivatives, revealing the practical electron-donating ability and providing additional active sites for further oxidation [40]. However, more detailed insight behaviors have not been elucidated yet. Herein, we demonstrate that the *para*-amino-substituted **TPA** derivatives can possess remarkable stability for the long-term requirement. In Scheme 1, **TPA-1N**, **TPA-2N**, and **TPA-3N** were designed and prepared to compare the correlation between the number of amino substituents and the EC behaviors. In addition, one of the amino substituents was modified to a dimethylamino group in **TPA-ADM**; the more stable and effective electron-donating ability results in enhanced EC performance than **TPA-2N**. Compared with the traditional work that connected several **TPA** units at *para*-orientation [17,41], this study provides a much more straightforward method to prepare the electrochromophores with multi-oxidation states. Moreover, the high optical contrast ratio, fast switching response speed, low oxidation potential, and long-term stability of these *para*-amino-substituted **TPA** derivatives confirm this facile and feasible approach for fabricating more efficient ECDs.

2. Results and discussion

2.1. Monomer synthesis and characterization

To realize the correlation among the number of amino-substituents, stability, and EC performance, four *para*-amino-substituted **TPA** were synthesized and investigated in this study. **TPA-1N**, **TPA-2N**, and **TPA-3N** were prepared according to the previous reports [17,42,43]. The detailed synthesis procedures of the new compound, **TPA-ADM**, are described in Supporting Information. The precursor nitro derivative **TPA-NDM** was obtained via Ullmann condensation between *4*-bromoanisole and *4*-dimethylamino-*4′*-nitrodiphenylamine. After the following Pd/C catalyzed reduction, **TPA-ADM** was successfully synthesized. The characterizations of **TPA-NDM** and **TPA-ADM** were confirmed by IR and NMR spectroscopies and illustrated in Figs. S1-S11. In Fig. S1, **TPA-NDM** showed the characteristic absorption of NO_2 stretching peaks at 1589 and 1309 cm^{-1}. After hydrogenation, the peaks of NO_2 stretching disappeared, and the generated NH_2 peaks for the stretching and bending characteristic absorption could be observed at 3433 and 3330 cm^{-1}, and 1632 cm^{-1}, respectively. The peak assignment of ^1H–^1H COSY and ^1H–^{13}C HSQC spectra confirmed the excellent agreement with the expected structures. The detailed characterization was illustrated in the Experiment Section of Supporting Information.

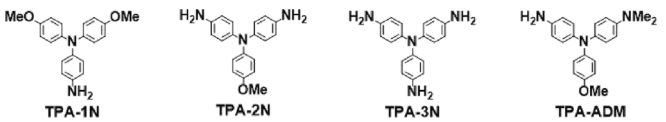

Scheme 1. Four designed and prepared *para*-amino-substituted **TPA** derivatives in this study.

2.2. Electrochemical and spectroelectrochemical properties

The electrochemical properties of **TPA-1N**, **TPA-2N**, **TPA-3N**, and **TPA-ADM** were investigated by cyclic voltammetry (CV) and spectroelectrochemistry conducted with the optically transparent thin-layer electrochemical (OTTLE) containing 0.5 μmol of **TPA**s in 1 mL of anhydrous γ-butyrolactone (GBL) and 0.1 M tetra-*n*-butylammonium perchlorate (TBAP) as the supporting electrolyte under nitrogen atmosphere. The CV diagrams of these four **TPA** derivatives are depicted in Fig. 1 and Figs. S12-S15, and the results are summarized in Table 1. **TPA-3N** showed the lowest first oxidation peaks at 0.34 V, which referred to the most substantial electron-donating ability and the resonance effect of IV-CT among the **TPA** center and three amino groups. With the continuous increase of applied potential, **TPA-3N** exhibited the second and third oxidation peaks at 0.73 and 1.73 V, indicating the extra redox active sites generated by the amino substituents. However, the excessive applied potential made the third oxidation unstable and irreversible. Therefore, the electrochemical and electrochromic studies would focus on the first two oxidation states for these **TPA** derivatives. In Fig. 1, the oxidation potential peaks of these **TPA** derivatives revealed identical sequences as the number of amino groups (**TPA-1N**: 0.52/0.98 V; **TPA-2N**: 0.43/0.79 V; **TPA-3N**: 0.34/0.73 V), indicating that **TPA-3N** is more energy efficient with the lowest driving potential. Besides, by changing one of the amino substituents to the dimethylamino group, **TPA-ADM** displayed lower oxidation potentials at 0.38 and 0.73 V compared to **TPA-2N**, implying the more vital electron-donating ability of dimethylamino substituent. The reversibility of these **TPA** derivatives was also evaluated by the anodic and cathodic peak current ratio ($i_{p,a}/i_{p,c}$) [44], and the values revealed all close to 1, representing good reversibility at the first two oxidation states. Comparing the ratio of **TPA-1N**, **TPA-2N**, and **TPA-3N**, the value of **TPA-3N** is the closest to 1. The enhancement of the reversibility could be ascribed to the stabilized effect from the IV-CT between more active sites [32]. With more amino substituents joined to the conjugated system, the decay of the cation radical stability from the corresponding **TPA** derivatives could be inhibited.

The spectroelectrochemistry measurements of **TPA**s in the UV–Vis-NIR region are illustrated in Figs. S12-S15. The results revealed that **TPA-1N**, **TPA-2N**, **TPA-3N**, and **TPA-ADM** exhibited their characteristic absorption peaks at 301, 304, 309, and 307 nm in the neutral state, respectively, due to the increasing electron-donating ability (**TPA-1N** < **TPA-2N** < **TPA-ADM** < **TPA-3N**), resulting in a redshift of the absorption peaks. For **TPA-1N**, as the applied potential increased to the first oxidation state of 0.7 V, four new characteristic peaks appeared at 367, 587, 713, and 794 nm, while the intensity of the original peak in the neutral state (301 nm) decreased. According to the previous study, the absorption spectrum for the trimethoxy-substituted **TPA** (**TPA-3OMe**, without additional effective redox-active sites) cation radical manifested three characteristic peaks at 386, 619, and 724 nm [45]. In comparison, for **TPA-1N**, the absorption peaks at 367 nm and two shoulders at 587 and 713 nm should belong to the absorption of the **TPA** cation radical, indicating that the first electron removal should occur on the **TPA** nitrogen center. Moreover, a new prominent absorption peak appeared at 794 nm, implying the intensive IV-CT absorption between the **TPA** center and amino substituent, similar to the previous reports [46]. When the potential increased to the second oxidation state (1.1 V), the peaks at 367, 713, and 794 nm would decrease, while the intensity raised at the height of 587 nm attributed to the primary absorption of dication [**TPA-1N**]$^{2+}$. For **TPA-2N** and **TPA-3N**, as the applied potential increased to the first oxidation state (0.6 V), **TPA-2N** exhibited the first oxidation peaks at 376 and 882 nm, while **TPA-3N** showed the first oxidation peaks at 387 and 851 nm. These two **TPA** derivatives displayed their IV-CT bands with longer wavelengths in the NIR region than **TPA-1N**, indicating the effect of donating ability from the additional amino

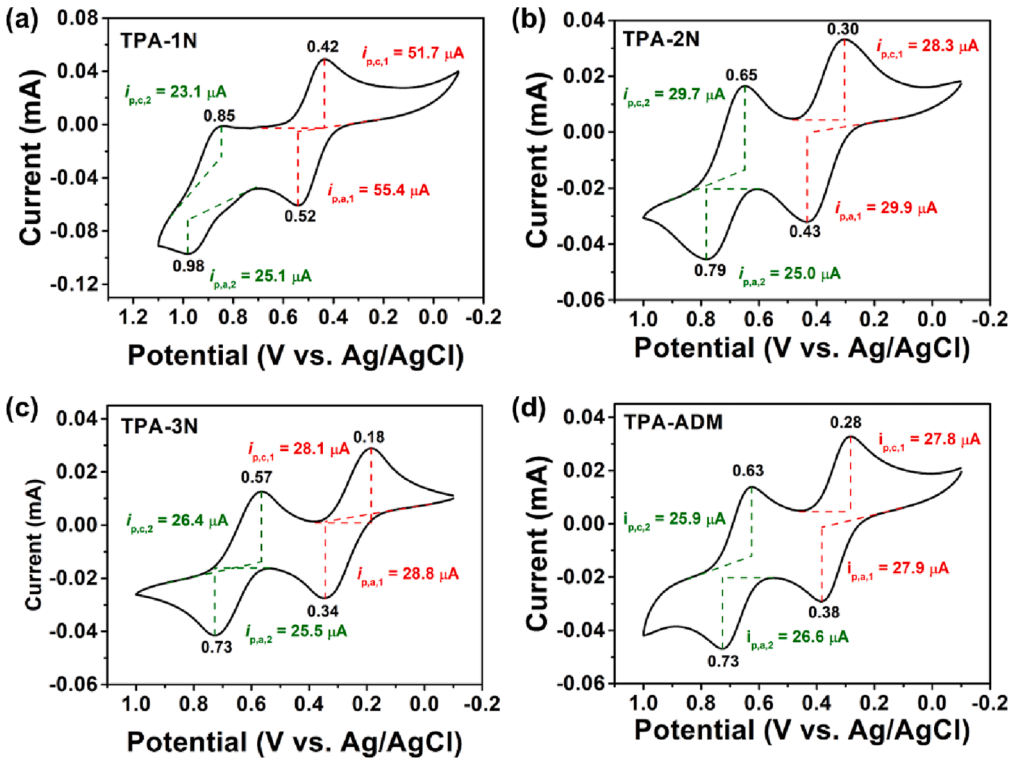

Fig. 1. Cyclic voltammetry diagrams of (a) **TPA-1N**, (b) **TPA-2N**, (c) **TPA-3N**, and (d) **TPA-ADM** conducted with platinum net in OTTLE cell at a scan rate of 50 mV/s. (sample amount: 0.5 μmol (5×10^{-4} M) in 1 mL of 0.1 M TBAP/GBL).

Table 1
The oxidation potential of **TPA**s of the first two oxidation states.

Index	1st oxidation state			2nd oxidation state		
	$E_{p,a}$ [V] [a]	$E_{p,c}$ [V] [b]	$i_{p,a}/i_{p,c}$ [c]	$E_{p,a}$ [V] [a]	$E_{p,c}$ [V] [b]	$i_{p,a}/i_{p,c}$ [c]
TPA-1N	0.52	0.42	1.07	0.98	0.85	1.08
TPA-2N	0.43	0.30	1.06	0.79	0.65	0.84
TPA-3N	0.34	0.18	1.02	0.73	0.57	0.97
TPA-ADM	0.38	0.28	1.00	0.73	0.63	1.03

[a] Anodic peak potential (oxidation). [b] Cathodic peak potential (reduction). [c] Peak current ratio, $i_{p,a}/i_{p,c} = 1$ for reversible redox system.

substituents. When the potential raised to the second oxidation potential of **TPA-2N** (0.9 V), two new characteristic peaks appeared at 602 and 734 nm, while the absorption intensity of the IV-CT band at 882 nm retained near the same value. The phenomenon might indicate that IV-CT is preserving between the two oxidized centers and the remaining neutral one. After fully oxidized, the IV-CT bands at 882 nm disappeared, and two characteristic peaks at 602 and 734 nm enhanced to higher values. Comparing the absorptions for the second and third oxidation states of **TPA-1N**, **TPA-2N**, and **TPA-3N**, we found that the absorbance and the wavelength increased as the number of amino substituents increased. Therefore, the amino group played a vital auxochrome role in enhancing absorption. **TPA-ADM** showed the characteristic peaks of first oxidation at 378 and 951 nm. Replacing the original amino substituent with a dimethyl amino group should typically cause the large redshift and board absorption band at 951 nm of IV-CT because the resonance structures would be more stable. Thus, the cation radical delocalized between the **TPA** center and dimethylamino group rather than the amino substituent. Because of the intensive mix-valance ability between the dimethylamino group and **TPA** center nitrogen, the second oxidation should be located on the amino group, creating a strong absorption peak at 747 nm. When the applied potential raised to the third oxidation, the absorption band of IV-CT at 951 nm diminished while the absorption peak at 747 nm was maintained at the same absorbance. The optical parameters of these amino-substituted **TPA**s are summarized in Table S1. In addition, the extinction coefficient of the prepared **TPA**s in the NIR region (ε_{NIR}) revealed that the value would increase from 14.0×10^3 M^{-1} cm^{-1} to 29.7×10^3 M^{-1} cm^{-1} as the more amino substituents in the **TPA** unit. **TPA-ADM** exhibited higher ε_{NIR} and ε_{visble} values than **TPA-2N** at the first and second oxidation states due to the strong resonance between the non-oxidized dimethylamino group and oxidized **TPA** cation radical. Upon the third oxidation state, **TPA-2N** would show much higher ε_{NIR} and ε_{visble} values to **TPA-ADM**, implying that the oxidized dimethylamino group attributed less absorbance than the oxidized amino group. Interestingly, **TPA-3N** revealed the highest ε value either in visible or NIR region at each oxidation state when compared to the others, implying that the **TPA** chromophores would possess high contrast just by introducing more amino groups even in low concentration.

2.3. Redox kinetics of TPAs

To further clarify the correlation between the molecular dynamics and amino groups, the kinetic studies of **TPA**s were used to calculate the diffusion coefficient (D, $cm^2 \cdot s^{-1}$) by Randles–Sevcik equation [47]. To estimate the D of the **TPA**s, a series of CV measurements with different scan rates were conducted, as illustrated in Fig. S16. The obtained peak current i_p was plotted with the square root of scan rate ($\nu^{0.5}$), and the linear regression slope gives the value of $i_p - \nu^{0.5}$, which could be converted to diffusion coefficient (D). The high linearity of the plots of $i_p - \nu^{0.5}$ suggested a diffusion-controlled reaction for the redox process [48]. The calculated diffusion coefficients (D) are summarized in Table S2. **TPA-3N** revealed the highest diffusion coefficient among all the **TPA** derivatives ($D_a = 9.65 \times 10^{-7}$ cm^2/s, $D_c = 6.25 \times 10^{-7}$ cm^2/s), which might be ascribed to the smaller hydrodynamic radii of the amino substituent in comparison to methoxy group. It is worth noting that the diffusion coefficients for the cation radicals are all smaller than the

corresponding neutral state species, implying that the cation radicals should form as the ion pair with the counter ion in the solution and slower the diffusion rate [49,50]. Furthermore, the electrochemical rate constant (k_{ox} and k_{red}) could also be calculated by Nicholson dimensionless number (ψ) and the obtained D according to the reference [51–54]. As shown in Fig. S17 and Table S2, the **TPA-3N** exhibited the most rapid rate either in oxidation or reduction compared to others, indicating that the multi-amino substituted **TPA** could efficiently enhance the electron transfer rate upon the redox process. Besides, by comparing with the **TPA-2N** and **TPA-ADM**, **TPA** attached with the amino group (**TPA-2N**: $k_{ox} = 6.65 \times 10^{-4}$; $k_{red} = 5.51 \times 10^{-4}$) displayed a higher rate constant than the dimethylamino group (**TPA-ADM**: $k_{ox} = 6.38 \times 10^{-4}$; $k_{red} = 4.90 \times 10^{-4}$), confirming the amino group possessed more efficient and rapid electron transfer than the dimethylamino group.

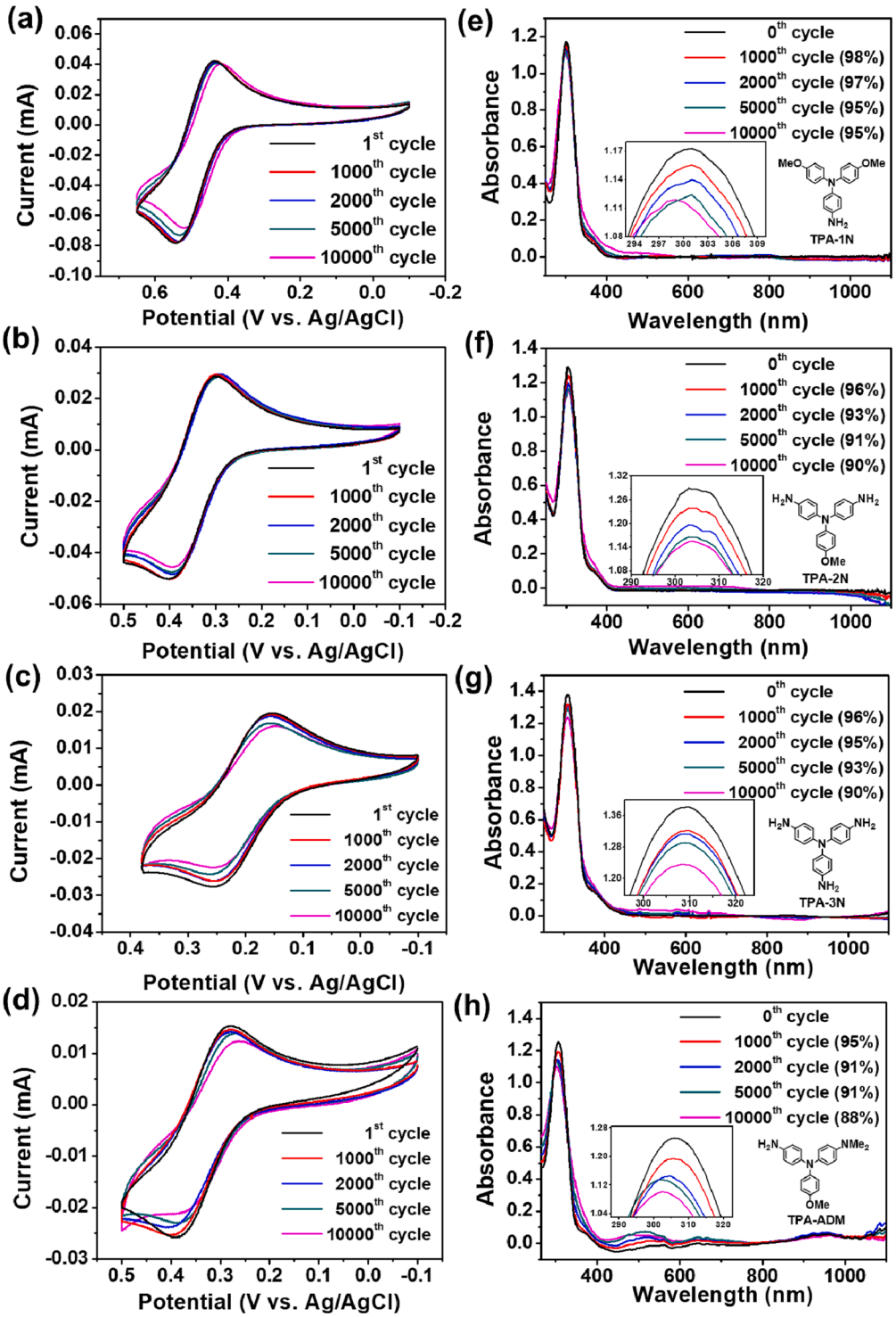

Fig. 2. The cyclic stability of (a) **TPA-1N** (b) **TPA-2N** (c) **TPA-3N** (d) **TPA-ADM** (sample amount: 0.5 μmol in 1 mL of 0.1 M TBAP/GBL) conducted with a platinum net in 0.1 M TBAP/GBL at the scan rate of 100 mV/s; The absorption spectra and recovery rate of (e) **TPA-1N**, (f) **TPA-2N**, (g) **TPA-3N**, and (h) **TPA-ADM** after different cycles of scanning.

2.4. Cycling stability of TPAs

The long-term stability of these **TPA**s was determined by continuous CV measurement up to ten thousand cycles in Fig. 2. For every thousand cycles of CV scanning, the cell would be applied a voltage of − 0.1 V to recover the electroactive species to the neutral state. An absorption spectrum was then recorded to evaluate the decay of the sample. The reversibility was calculated by the remained absorbance after CV scans divided by the initial absorbance. All these **TPA** derivatives demonstrated outstanding electrochemical stability after long-term experiments. No obvious current decay could be noticed even after ten thousand cycles in Fig. 2a-d. For the absorption spectra in Fig. 2e-h, the calculated electrochemical reversibility after ten thousand cycles were **TPA-1N**: 95%, **TPA-2N**: 90%, **TPA-3N**: 90%, and **TPA-ADM**: 88%. The incredible reversibility of these **TPA** derivatives suggests that most of the cation radicals of **TPA**s could recover to the original neutral state even after long-term switching experiments, demonstrating high feasibility in the further application.

2.5. EC behaviors of liquid-type ECDs

The liquid-type devices were fabricated to elucidate the electrochemical behaviors and feasibility of this *para*-amino substituted **TPA** derivatives for long-term application. The detailed procedures are described in Supporting Information and Fig. S18. The ECDs based on **TPA** derivatives were fabricated by incorporating heptyl viologen (**HV**) as the complementary electrochromic materials, which can lower the oxidation potential and provide complementary absorption peaks to enhance the contrast ratio of the ECDs [55–57]. Each device contained 0.72 μmol **TPA**s (0.015 M), 0.72 μmol **HV** (0.015 M), and 4.8 μmol $TBABF_4$ (0.1 M) in 0.048 mL GBL with a 2 × 2 cm^2 active area. The CV diagrams and the parameters of the ECDs are illustrated and summarized in Fig. S19 and Table 2. **TPA-3N/HV** possessed the lowest oxidation potentials at 0.70 and 1.46 V for the first and second oxidation states among all ECDs. The oxidation potentials of the ECDs revealed the same sequence as the related **TPA** derivatives of the solution sample in OTTLE measurement, where the oxidation potential decreased as the electron-donating effect increased (**TPA-1N/HV**: 0.95/1.84 V; **TPA-2N/HV**: 0.83/1.60 V; **TPA-ADM/HV**: 0.78/1.55 V; **TPA-3N/HV**: 0.70/1.46 V). Previous research demonstrated that the oxidation redox process of **TPA/TPA**$^{\bullet+}$ could be assisted with the reduction of **HV**$^{2+}$/**HV**$^{\bullet+}$ [58]. However, a prominent redox couple of **HV**$^{\bullet+}$/**HV**$^{2+}$ with residue color appeared at −0.06/0.06 V in **TPA-1N/HV** device, implying the unrecovered **HV**$^{\bullet+}$ after the assisted reduction process.

The EC properties of the devices were investigated by spectroelectrochemistry analysis, illustrated in Fig. 3. For **TPA-1N/HV**, the first oxidation state of the device involved the oxidation of **TPA-1N** to **TPA-1N**$^{\bullet+}$ and the reduction of **HV**$^{2+}$ to **HV**$^{\bullet+}$. Consequently, the characteristic peaks were the superposition of **HV**$^{\bullet+}$ appeared around 400 and 600 nm (Fig. S20) [17,56], and **TPA-1N**$^{\bullet+}$ appeared at 794 nm when the applying potential raised to 1.2 V. Afterwards, the formation of **TPA-1N**$^{2+}$ would generate a new characteristic peak around 580 nm, accompanied by a decrease of absorption at 794 nm as the potential was further increasing to 2.0 V. Similar results could be observed in the rest ECDs, where **TPA-2N/HV** showed three characteristic peaks at 400, 608, and 884 nm at the first oxidation state (0.9 V), revealing the formation of **TPA-2N**$^{\bullet+}$ and **HV**$^{\bullet+}$. At the second oxidation state of **TPA-2N/HV** (1.8 V), the formation of **TPA-2N**$^{2+}$ would generate another characteristic peak at 733 nm. For **TPA-3N/HV**, the distinct peaks of the first oxidation state (0.9 V) appeared at 400, 608, and 853 nm. Because **TPA-3N**$^{2+}$ revealed almost no absorption between 450 and 600 nm, the absorption of 608 nm could retain the same value at the second oxidation state, implying the formation of **HV**$^{\bullet+}$ was saturated at the first oxidation state for the ECDs. The absorption spectra of **TPA-ADM/HV** followed a similar evolution as the other ECDs mentioned earlier. However, it showed a red shift up to 953 nm with a high extinction coefficient of 11.67 × 10^{-3} M cm^{-1}, resulting from the strong auxochrome of the dimethylamine group. Additionally, **TPA-3N/HV** also revealed a high absorbance in the NIR region with only 0.72 μmol of **TPA-3N**, implying an excellent chromophore as EC material in high-contrast NIR devices.

Table 2
Electrochemical properties of the prepared ECDs.

Index	1st oxidation state			2nd oxidation state	
	$E_{p,a}$ [V] [a]	$E_{p,c}$ [V] [b]	$i_{p,a}/i_{p,c}$ [c]	$E_{p,a}$ [V] [a]	$E_{p,c}$ [V] [b]
TPA-1N/HV	0.95	0.70	1.10	1.84	1.53
TPA-2N/HV	0.83	0.55	1.20	1.60	1.34
TPA-3N/HV	0.70	0.44	1.06	1.46	1.24
TPA-ADM/HV	0.78	0.53	1.20	1.55	1.30

[a] Anodic peak potential (oxidation). [b] Cathodic peak potential (reduction). [c] Peak current ratio, $i_{p,a}/i_{p,c} = 1$ for reversible redox system.

The CIELAB color space parameters were adapted to quantify the color change for the ECDs during the redox process. The ECDs appearance and the corresponding L*a*b* values are depicted in Figs. S21-S24 and presented as videos in Supporting Information. With the incorporation of **HV**, the absorption merging near 600 nm of **HV** with **TPA**s could enhance optical contrast. For **TPA-1N/HV**, the device exhibited a transparent and colorless appearance at the neutral state (L*: 97.52, a*: −0.20, b*: 4.67). After oxidation, the device revealed a navy-blue appearance (L*: 47.90, a*: 5.66, b*: −55.12) at the first oxidation state (1.2 V), and then the color became denser (L*: 31.09, a*: 2.15, b*: −44.40) at the second oxidation state (2.0 V). A similar color change could also be observed for other ECDs. For **TPA-2N/HV**, the color changes from colorless (L*: 98.23, a*: 1.26, b*: 2.69) to blue (L*: 69.29, a*: −6.76, b*: −37.93) and then deeper blue (L*: 61.21, a*: −9.44, b*: −26.39); **TPA-3N/HV** displayed different colors during the oxidation process from transparent and colorless (L*: 97.90, a*: 1.08, b*: 2.68) to cobalt blue (L*: 55.69, a*: −8.92, b*: −46.47) and then dark blue (L*: 42.90, a*: −12.80, b*: −45.93); The appearance of **TPA-ADM/HV** varied from colorless (L*: 97.87, a*: −1.08, b*: 6.72) to dark azure (L*: 53.50, a*: −26.93, b*: −37.61) and then gray blue (L*: 47.57, a*: −34.86, b*: −35.81).

The efficacies of the ECDs were further determined with the time-depending measurement. The coloration efficiency (η_{CE}) is an essential factor in deciding the coloring ability for an ECD under a certain amount of charge consumption, which the following equation could calculate:

$$\eta_{CE} = \frac{\Delta OD}{Q} \quad (1)$$

where ΔOD is the change in optical density, defined as $\Delta OD = \log [T_b/T_c]$, T_b and T_c are the transmittances of bleaching and coloring states, respectively, and Q is the consumed charge density that is integral from i-t curve. The plots of ΔOD determined the coloration efficiency (η_{CE}) of the ECDs under different amounts of consumed charge density (Q), and the plots are illustrated in Fig. 4a and S25. The linear regression slope at the beginning of the plots represented the coloration efficiency (η_{CE}) of the ECDs. **TPA-3N/HV** possessed the highest η_{CE} (631 cm^2/C) among the four devices, implying the highest ΔOD in the same charge consumption and energy efficiency. For other ECDs, the charge consumptions were approximately the same, so the η_{CE} was determined by the optical difference during the coloration process. **TPA-1N/HV** showed the lowest η_{CE} (189 cm^2/C) due to the lowest contrast; **TPA-2N/HV** (418 cm^2/C) and **TPA-ADM/HV** (452 cm^2/C) revealed similar η_{CE} based on the similar ΔOD around 1.1 to 1.2. Furthermore, according to the first oxidation potentials obtained from the CV diagrams, the coloring voltages were chosen as 1.2 V, and the bleaching voltages were set as − 0.3 V for **TPA-1N/HV** and 0.9 V for the other ECDs to evaluate the response capability of the prepared ECDs. The coloring time (t_c) and bleaching time (t_b) are defined as the moment for reaching 90% of the maximum

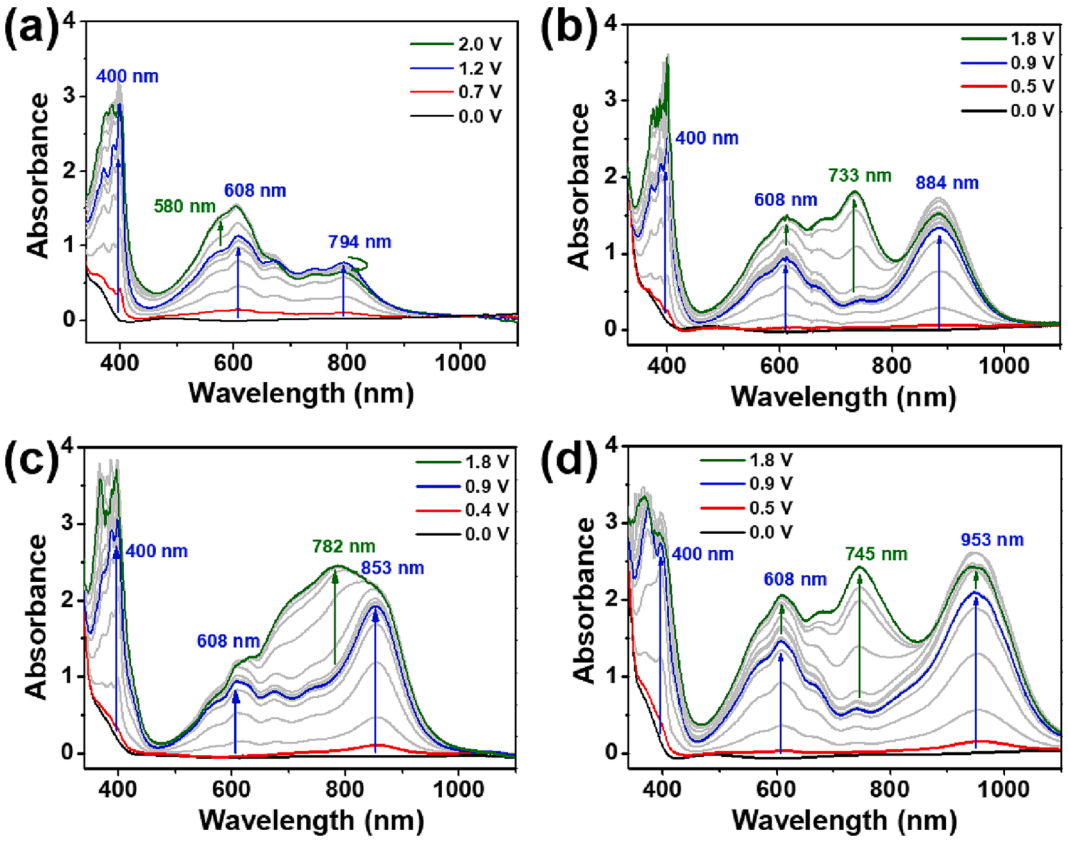

Fig. 3. Spectroelectrochemistry diagrams of (a) **TPA-1N/HV**, (b) **TPA-2N/HV**, (c) **TPA-3N/HV**, and (d) **TPA-ADM/HV** ECDs. The devices were fabricated from ITO glass with a 2 × 2 cm^2 active area, containing 0.72 μmol **TPAs** (0.015 M), 0.72 μmol **HV** (0.015 M), and 4.8 μmol $TBABF_4$ (0.1 M) in 0.048 mL GBL.

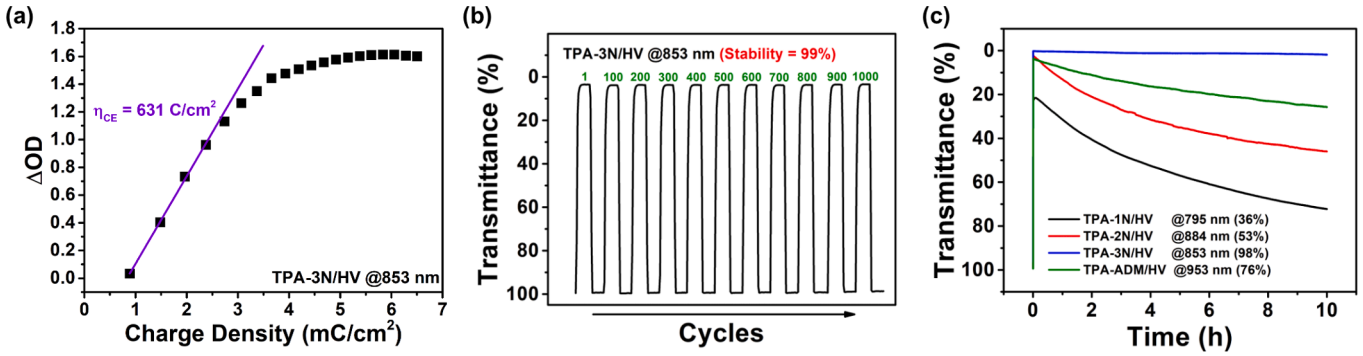

Fig. 4. (a) Coloration efficiency (η_{CE}) of **TPA-3N/HV**. (b) Switching stability of **TPA-3N/HV** for 1000 cycles with 60 s cycle time, 0.9 V as the coloring voltages, and − 0.3 V as the bleaching voltage. (c) Long-term stability of ECDs at the on-state for 10 h. The devices were derived from ITO glass with a 2 × 2 cm^2 active area, containing 0.72 μmol **TPAs** (0.015 M), 0.72 μmol **HV** (0.015 M), and 4.8 μmol $TBABF_4$ (0.1 M) in 0.048 mL GBL.

transmittance difference during oxidation or reduction. The switching response behaviors for the ECDs depicted in Fig. 5 demonstrate that the t_c would significantly decrease from 4.6 s to 1.9 s among four ECDs by introducing more amino groups in the **TPA** unit. In contrast, the device derived from **TPA-ADM/HV** with dimethylamino group showed the same t_c as **TPA-2N/HV**. In addition, the coloration speed (υ_c) and optical coloration rate constant (k_c) could be calculated, as shown and tabulated in Fig. S26 and Table 3 and Table S4, respectively [59]. The results displayed that **TPA-3N/HV** possessed the highest values of 46.4 % s^{-1} and 0.593 s^{-1} for υ_c and k_c, respectively. Besides, among the prepared ECDs, the larger values of υ_c and k_c exhibited a shorter t_c along with the more amino group substituted in the **TPA** unit, indicating the same trend as the diffusivity and electrochemical rate constant study mentioned above. Besides, according to the Nicholson dimensionless number (ψ) in Fig. S17, **TPA-3N** showed the largest k_{ox}, implying the rapid electron transfer during the coloring process. Based on this result, the faster t_c could also be attributed to the rapid electron transfer. However, the t_b exhibited a more prolonged time needed to bleach from the coloring state, along with more amino groups in the **TPA** unit (from 3.2 s to 4.2 s). This phenomenon conflicted with our above kinetic studies that the D_c and k_{red} of **TPA-3N** exhibited the highest values, which should reflect the shortest t_c. The longer t_b for **TPA-3N/HV** would probably be attributed to the more intensive switching optical contrast that needs more time to be erased. Similarly, **TPA-2N/HV** and **TPA-ADM/HV** exhibited relatively long t_b (3.7 s and 4.1 s) while with higher D_c and k_{red} values compared to **TPA-1N/HV**.

The electrochemical stability of the ECDs is crucial and was elucidated with the continuous switching cycling under their coloring/

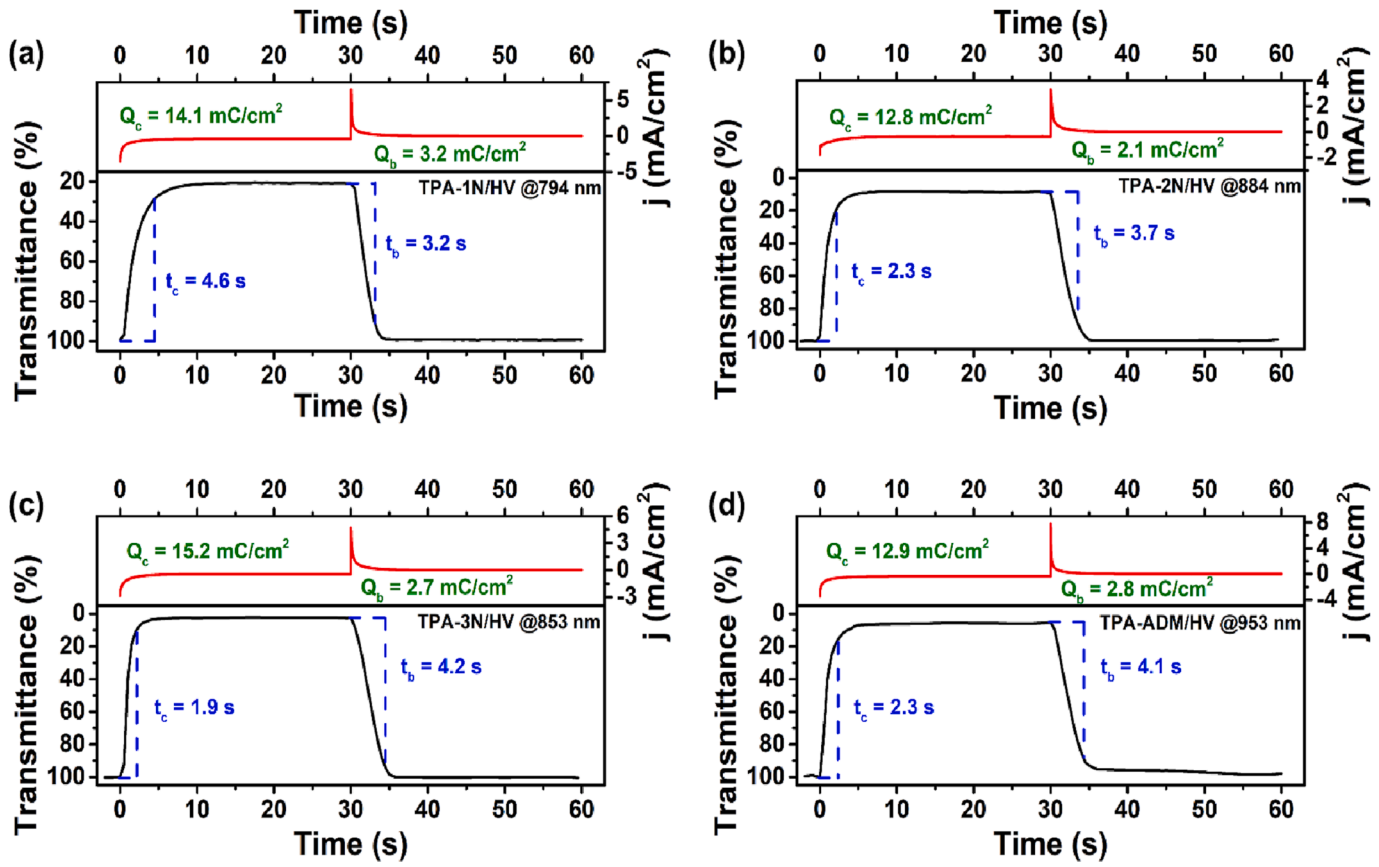

Fig. 5. Response time and injected charge plots of (a) **TPA-1N/HV**, (b) **TPA-2N/HV**, (c) **TPA-3N/HV**, and (d) **TPA-ADM/HV**. The coloring voltages were 1.2 V for **TPA-1N/HV** and 0.9 V for the others, while the bleaching voltages were − 0.3 V for all the devices with 60 s cycle time. The devices were fabricated from ITO glass with a 2 × 2 cm^2 active area, containing 0.72 μmol **TPAs** (0.015 M), 0.72 μmol **HV** (0.015 M), and 4.8 μmol $TBABF_4$ (0.1 M) in 0.048 mL GBL.

bleaching potentials. The results are depicted in Fig. 4b, Figs. S27-S28, and summarized in Table 3. In the first one hundred cycles, **TPA-3N/HV** and **TPA-ADM/HV** exhibited superior stability for only 1% and 3% decay of ΔT (stability: 99% and 97%); more scan cycles with extended experiments for these two ECDs were conducted. After one thousand switching cycles, **TPA-3N/HV** and **TPA-ADM/HV** also displayed remarkable stability for only 1% and 10% decay of ΔT (stability: 99% and 90%). In addition, **TPA-3N/HV** was also measured for the 100-cycle switching stability after 5000 or 10,000 cycles of CV scans, shown in Fig. S29. The results indicated that **TPA-3N/HV** could maintain the stability of 96.2% and 94.6% after 5000 and 10,000 cycles, respectively. The results suggested that **TPA-3N/HV** would be an ultra-stable ECD under this applied potential window (−0.3/0.9 V). The practical long-term stability of these ECDs was further recorded in Fig. 4c. After giving the corresponding coloring potentials for ten hours, **TPA-3N/HV** could keep 98% of its maximum transmittance contrast, implying the most electrochemically stable at the first oxidation state among all the **TPA** derivatives. Based on these results, we proposed that owing to having more auxochrome of the amino groups in **TPA-3N**, the oxidized nitrogen center has three electroactive sites to resonance by the IVCT effect. Thus **TPA-3N/HV** performed with remarkable stability. Furthermore, by comparison of the representative EC characteristics of other reported small molecules ECDs summarized in Table S5 and Fig. 6, the **TPA-3N/HV** derived from the unprecedented facile, energy-saving, economic-competitive approach demonstrates superior performance of high coloration efficiency (631C/cm^2) and optical contrast (ΔT = 98%) in the NIR region while preserving high stability (t_c = 1.9 s) and fast response speed (46.4 % s^{-1}) [18,26,60–63].

3. Conclusions

Four *para*-amino-substituted **TPA** derivatives, **TPA-1N**, **TPA-2N**, **TPA-3N**, and **TPA-ADM**, have been prepared and investigated the correlation between the amino substituents and the electrochemical/

Table 3
The electrochromic parameters of ECDs.

Index	t_c [s] [a]	t_b [s] [b]	ΔT [%] [c]	η_{CE} [cm^2/C] [d]	v_c [%·s^{-1}] [e]	Stability		
						100 cycles	1000 cycles	10 h
TPA-1N/HV	4.6	3.2	79	189	15.5	84%	–	36%
TPA-2N/HV	2.3	3.7	91	418	35.6	92%	–	53%
TPA-3N/HV	1.9	4.2	98	631	46.4	99%	99%	98%
TPA-ADM/HV	2.3	4.1	93	452	36.4	97%	90%	76%

[a] Coloring time from the bleaching state to 90% of total transmittance change. [b] Bleaching time from the coloring state to 90% of complete transmittance change. [c] Change in transmittance is defined as $\Delta T = T_b - T_c$, where T_b and T_c are the transmittances of bleaching and coloring states, respectively. [d] Coloration efficiency is determined by the slope of change in optical density (ΔOD) versus charge density. Change in optical density is defined as $\Delta OD = \log [T_b/T_c]$.
[e] Coloration response speed, defined as 90% of ΔT divided by t_c.

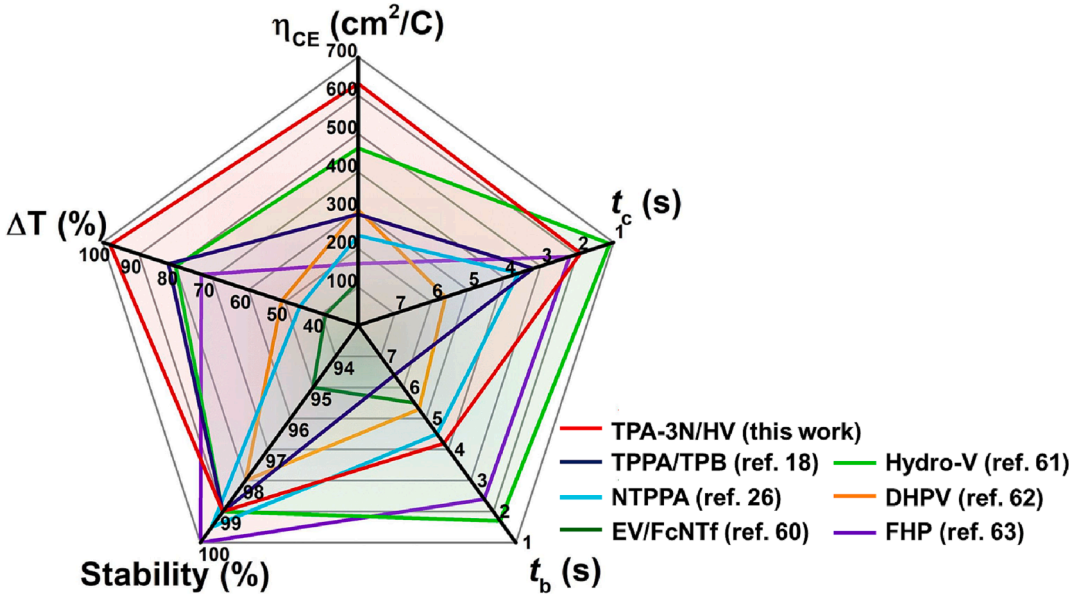

Fig. 6. Comparison of electrochromic parameters of reported small molecules ECDs. The stability of the ECDs was determined with the percent of remaining ΔT after 1000 switching cycles, excluding TPPA/TPB (32 hr, on-state) and FHP (5000 cycles). The electrolyte for each ECD contains TPPA/TPB: 0.04 M HV and 0.16 M $TBABF_4$ in 0.05 mL PC/GBL (1/1) [18]. NTPPA: 0.015 M HV in 0.05 mL GBL [26]. EV/FcNTf: 50 mM [BMIm][NTf_2] [60]. Hydro-V: composting only DMF as solvent [61]. DHPV: 5 mg Fc, 200 mg PC, 200 mg $C_2F_6LiNO_4S_2$, 2 mL methanol, and 400 mg PVB [62]. FHP: 0.12 mM Fc, 150 mg PC, 160 mg LiTFSI, 1.5 mL methanol, and 300 mg PVB [63].

electrochromic properties. The introduction of amino substituents could reduce the oxidation potential significantly and generate extra oxidation states that enrich the color evolution, fast diffusivity, and rapid electron transfer, resulting in low-energy consumption materials. These **TPA** derivatives also present remarkable reversibility for more than 88% after ten thousand cycles of uninterrupted CV measurement. The related ECDs with the complement of HV reveal exceptional EC performance, where **TPA-3N/HV** demonstrates the lowest oxidation potential (0.70 V), the shortest coloring time (1.9 s), the highest coloration efficiency (631 cm^2/C), and the most superior stability (99% for 1000 cycles, 98% for 10-hour coloring). This unprecedented study proves that the multi-*para*-amino-substituted **TPA** derivatives can exhibit outstanding EC behaviors with exceptional switching stability, providing a facile approach to preparing energy-efficient and high-performance ECDs.

Declaration of Competing Interest

The authors declare that they have no known competing financial interests or personal relationships that could have appeared to influence the work reported in this paper.

Data availability

No data was used for the research described in the article.

Acknowledgments

This work received financial support from the National Science and Technology Council in Taiwan (NSTC 111-2113-M-002-024 and 111-2221-E-002-028-MY3). The authors gratefully thank Ms. Chiu-Hui He in the Instrumentation Center at NTNU for assistance in NMR measurements and Ms. Ching-Wei Lu and Ms. Shu-Yun Sun in the Instrumentation Center at NTU (elementar vario EL cube and Orbitrap QE Plus Mass Spectrometry) for assistance in EA and ESI-MS measurements.

Appendix A. Supplementary data

Supplementary data to this article can be found online at https://doi.org/10.1016/j.cej.2023.143003.

References

[1] R.J. Mortimer, Electrochromic materials, Chem. Soc. Rev. 26 (3) (1997) 147–156, https://doi.org/10.1039/CS9972600147.
[2] W. Wu, M. Wang, J. Ma, Y. Cao, Y. Deng, Electrochromic metal oxides: recent progress and prospect, Adv. Electron. Mater. 4 (8) (2018) 1800185, https://doi.org/10.1002/aelm.201800185.
[3] Y. Wang, E.L. Runnerstrom, D.J. Milliron, Switchable materials for smart windows, Annu. Rev. Chem. Biomol. Eng. 7 (2016) 283–304. 10.1146/annurev-chembioeng-080615-034647.
[4] J. Niu, Y. Wang, X. Zou, Y. Tan, C. Jia, X. Weng, L. Deng, Infrared electrochromic materials, devices and applications, Appl. Mater. Today 24 (2021) 101073, https://doi.org/10.1016/j.apmt.2021.101073.
[5] C. Gu, A.B. Jia, Y.M. Zhang, S.X.A. Zhang, Emerging electrochromic materials and devices for future displays, Chem. Rev. 122 (18) (2022) 14679–14721, https://doi.org/10.1021/acs.chemrev.1c01055.
[6] R.J. Mortimer, Organic electrochromic materials, Electrochim. Acta 44 (18) (1999).
[7] A. Tsuboi, K. Nakamura, N. Kobayashi, Multicolor electrochromism showing three primary color states (Cyan–Magenta–Yellow) based on size- and shape-controlled silver nanoparticles, Chem. Mater. 26 (22) (2014) 6477–6485. 10.1021/cm5039039.
[8] K. Wang, J.W. Steeds, Z. Li, Y. Tian, Photoluminescence studies of growth-sector dependence of nitrogen distribution in synthetic Ib diamond, Mater. Charact. 94 (2014) 14–18, https://doi.org/10.1016/j.matchar.2014.04.010.
[9] B.H. Chen, S.Y. Kao, C.W. Hu, M. Higuchi, K.C. Ho, Y.C. Liao, Printed multicolor high-contrast electrochromic devices, ACS Appl. Mater. Interfaces 7 (45) (2015) 25069–25076, https://doi.org/10.1021/acsami.5b08061.
[10] J.T.S. Allan, S. Quaranta, I.I. Ebralidze, J.G. Egan, J. Poisson, N.O. Laschuk, F. Gaspari, E.B. Easton, O.V. Zenkina, Terpyridine-based monolayer electrochromic materials, ACS Appl. Mater. Interfaces 9 (46) (2017) 40438–40445, https://doi.org/10.1021/acsami.7b11848.
[11] M. Wałęsa Chorab, R. Banasz, D. Marcinkowski, M. Kubicki, V. Patroniak, Electrochromism and electrochemical properties of complexes of transition metal ions with benzimidazole-based ligand, RSC Adv. 7 (80) (2017) 50858–50867, https://doi.org/10.1039/C7RA10451K.
[12] M.T. Kaczmarek, M. Skrobanska, M. Zabiszak, M. Wałęsa Chorab, M. Kubicki, R. Jastrzab, Coordination properties of N, N'-bis(5-methylsalicylidene)-2-hydroxy-1,3-propanediamine with d- and f-electron ions: crystal structure, stability in solution, spectroscopic and spectroelectrochemical studies, RSC Adv. 8 (54) (2018) 30994–31007, https://doi.org/10.1039/C8RA03565B.
[13] M. Yoshida, H. Shitama, W.M.C. Sameera, A. Kobayashi, M. Kato, Robust triplatinum redox-chromophore for a post-synthetic color-tunable electrochromic system, Chem. – A Eur. J. 25 (32) (2019) 7669–7678, https://doi.org/10.1002/chem.201900713.

[14] G. Cai, J. Chen, J. Xiong, A. Lee-Sie Eh, J. Wang, M. Higuchi, P.S. Lee, Molecular level assembly for high-performance flexible electrochromic energy-storage devices, ACS Energy Lett. 5 (4) (2020) 1159–1166.
[15] G. Cai, R. Zhu, S. Liu, J. Wang, C. Wei, K.J. Griffith, Y. Jia, P.S. Lee, Tunable intracrystal cavity in tungsten bronze-like bimetallic oxides for electrochromic energy storage, Adv. Energy Mater. 12 (5) (2022) 2103106.
[16] P. Lei, J. Wang, Y. Gao, C. Hu, S. Zhang, X. Tong, Z. Wang, Y. Gao, G. Cai, An electrochromic nickel phosphate film for large-area smart window with ultra-large optical modulation, Nano-Micro Lett. 15 (1) (2023) 34.
[17] J.T. Wu, T.L. Hsiang, G.S. Liou, Synthesis and optical properties of redox-active triphenylamine-based derivatives with methoxy protecting groups, J. Mater. Chem. C 6 (48) (2018) 13345–13351, https://doi.org/10.1039/C8TC05196H.
[18] J.T. Wu, G.S. Liou, A novel panchromatic shutter based on an ambipolar electrochromic system without supporting electrolyte, Chem. Commun. 54 (21) (2018) 2619–2622, https://doi.org/10.1039/C8CC00224J.
[19] Y. Sun, M. Shi, Y. Zhu, I.F. Perepichka, X. Xing, Y. Liu, C. Yan, H. Meng, Multicolored cathodically coloring electrochromism and electrofluorochromism in regioisomeric star-shaped carbazole dibenzofurans, ACS Appl. Mater. Interfaces 12 (21) (2020) 24156–24164, https://doi.org/10.1021/acsami.0c00883.
[20] K.W. Shah, S.X. Wang, D.X.Y. Soo, J. Xu, Viologen-based electrochromic materials: from small molecules, polymers and composites to their applications, Polymers 11 (11) (2019) 1839.
[21] Y. Zhang, X. Jin, W. Zhang, C. Gu, X. Liu, Y.M. Zhang, A bistable electrochromic device based on poly(viologen)s, Dyes Pigm. 209 (2023), https://doi.org/10.1016/j.dyepig.2022.110902.
[22] S.Y. Kao, H.C. Lu, C.W. Kung, H.W. Chen, T.H. Chang, K.C. Ho, Thermally cured dual functional viologen-based all-in-one electrochromic devices with panchromatic modulation, ACS Appl. Mater. Interfaces 8 (6) (2016) 4175–4184, https://doi.org/10.1021/acsami.5b11947.
[23] R. Vergaz, D. Barrios, J.M. Sánchez Pena, C. Pozo Gonzalo, M. Salsamendi, Relating cyclic voltammetry and impedance analysis in a viologen electrochromic device, Sol. Energy Mater. Sol. Cells 93 (12) (2009) 2125–2132, https://doi.org/10.1016/j.solmat.2009.08.009.
[24] H.J. Yen, G.S. Liou, Recent advances in triphenylamine-based electrochromic derivatives and polymers, Polym. Chem. 9 (22) (2018) 3001–3018, https://doi.org/10.1039/C8PY00367J.
[25] S.J. Yeh, C.Y. Tsai, C.Y. Huang, G.S. Liou, S.H. Cheng, Electrochemical characterization of small organic hole-transport molecules based on the triphenylamine unit, Electrochem. Commun. 5 (5) (2003).
[26] J.T. Wu, H.T. Lin, G.S. Liou, Synthesis and characterization of novel triarylamine derivatives with dimethylamino substituents for application in optoelectronic devices, ACS Appl. Mater. Interfaces 11 (16) (2019) 14902–14908, https://doi.org/10.1021/acsami.9b00402.
[27] S.Y. Chen, M.H. Pai, G.S. Liou, Effects of alkyl chain length and anion on the optical and electrochemical properties of AIE-active α-cyanostilbene-containing triphenylamine derivatives, J. Mater. Chem. C 8 (22) (2020) 7454–7462, https://doi.org/10.1039/D0TC00683A.
[28] M. Yano, Y. Ishida, K. Aoyama, M. Tatsumi, K. Sato, D. Shiomi, A. Ichimura, T. Takui, Synthesis and electronic properties of tetraaryl p- and m-phenylenediamines, Synth. Met. 137 (1) (2003) 1275–1276, https://doi.org/10.1016/S0379-6779(02)01137–2.
[29] H.J. Yen, S.M. Guo, G.S. Liou, Synthesis and unexpected electrochemical behavior of the triphenylamine-based aramids with ortho- and para-trimethyl-protective substituents, J. Polym. Sci. A Polym. Chem. 48 (23) (2010) 5271–5281, https://doi.org/10.1002/pola.24326.
[30] H.J. Yen, S.M. Guo, J.M. Yeh, G.S. Liou, Triphenylamine-based polyimides with trimethyl substituents for gas separation membrane and electrochromic applications, J. Polym. Sci. A Polym. Chem. 49 (16) (2011) 3637–3646, https://doi.org/10.1002/pola.24802.
[31] C. Lambert, G. Nöll, The class II/III transition in triarylamine redox systems, J. Am. Chem. Soc. 121 (37) (1999) 8434–8442, https://doi.org/10.1021/ja991264s.
[32] H.J. Yen, S.M. Guo, G.S. Liou, J.C. Chung, Y.C. Liu, Y.F. Lu, Y.Z. Zeng, Mixed-valence class I transition and electrochemistry of bis(triphenylamine)-based aramids containing isolated ether-linkage, J. Polym. Sci. A Polym. Chem. 49 (17) (2011) 3805–3816, https://doi.org/10.1002/pola.24819.
[33] H.J. Yen, G.S. Liou, Solution-processable novel near-infrared electrochromic aromatic polyamides based on electroactive tetraphenyl-p-phenylenediamine moieties, Chem. Mater. 21 (17) (2009) 4062–4070, https://doi.org/10.1021/cm9015222.
[34] Y.C. Kung, S.H. Hsiao, Fluorescent and electrochromic polyamides with pyrenylamine chromophore, J. Mater. Chem. 20 (26) (2010) 5481–5492, https://doi.org/10.1039/C0JM00495B.
[35] S.H. Cheng, S.H. Hsiao, T.H. Su, G.S. Liou, Novel aromatic poly(amine-imide)s bearing A pendent triphenylamine group: synthesis, thermal, photophysical, electrochemical, and electrochromic characteristics, Macromolecules 38 (2) (2005) 307–316, https://doi.org/10.1021/ma048774d.
[36] Y.C. Wang, Y.J. Shao, G.S. Liou, S. Nagao, Y. Makino, E. Akiyama, M. Kato, H. Shimomoto, E. Ihara, Synthesis and electrochromic properties of polyamines containing a 4,4'-diaminotriphenylamine-N, N'-diyl unit in the polymer backbone: Ru-catalyzed N-H insertion polycondensation of 1,4-phenylenebis(diazoacetate) with 4,4'-diaminotriphenylamine derivatives, Polym. Chem. 13 (46) (2022) 6369–6376, https://doi.org/10.1039/D2PY01118B.
[37] H.S. Liu, B.C. Pan, D.C. Huang, Y.R. Kung, C.M. Leu, G.S. Liou, Highly transparent to truly black electrochromic devices based on an ambipolar system of polyamides and viologen, NPG Asia Mater. 9 (6) (2017) e388, https://doi.org/10.1038/am.2017.57.
[38] F.W. Li, T.C. Yen, G.S. Liou, Synthesis of high-performance electrochromic material for facile fabrication of truly black electrochromic devices, Electrochim. Acta 367 (2021) 137474, https://doi.org/10.1016/j.electacta.2020.137474.
[39] H.J. Yen, G.S. Liou, Design and preparation of triphenylamine-based polymeric materials towards emergent optoelectronic applications, Prog. Polym. Sci. 89 (2019) 250–287, https://doi.org/10.1016/j.progpolymsci.2018.12.001.
[40] K. Yuan Chiu, T. Xiang Su, J. Hong Li, T.H. Lin, G.S. Liou, S.H. Cheng, Novel trends of electrochemical oxidation of amino-substituted triphenylamine derivatives, J. Electroanal. Chem. 575 (1) (2005) 95–101, https://doi.org/10.1016/j.jelechem.2004.09.005.
[41] H.J. Yen, H.Y. Lin, G.S. Liou, Novel starburst triarylamine-containing electroactive aramids with highly stable electrochromism in near-infrared and visible light regions, Chem. Mater. 23 (7) (2011) 1874–1882. 10.1021/cm103552k.
[42] C.W. Chang, G.S. Liou, S.H. Hsiao, Highly stable anodic green electrochromic aromatic polyamides: synthesis and electrochromic properties, J. Mater. Chem. 17 (10) (2007) 1007–1015. 10.1039/B613140A.
[43] G.S. Liou, C.W. Chang, Highly stable anodic electrochromic aromatic polyamides containing N,N,N',N'-tetraphenyl-p-phenylenediamine moieties: synthesis, electrochemical, and electrochromic properties, Macromolecules 41 (5) (2008) 1667–1674. 10.1021/ma702146h.
[44] Y.R. In, Y.M. Kim, Y. Lee, W.Y. Choi, S.H. Kim, S.W. Lee, H.C. Moon, Ultra-low power electrochromic heat shutters through tailoring diffusion-controlled behaviors, ACS Appl. Mater. Interfaces 12 (27) (2020) 30635–30642, https://doi.org/10.1021/acsami.0c05918.
[45] W.H. Chen, F.W. Li, G.S. Liou, Novel stretchable ambipolar electrochromic devices based on highly transparent AgNW/PDMS hybrid electrodes, Adv. Opt. Mater. 7 (19) (2019) 1900632, https://doi.org/10.1002/adom.201900632.
[46] S.H. Hsiao, G.S. Liou, Y.C. Kung, H.J. Yen, High contrast ratio and rapid switching electrochromic polymeric films based on 4-(dimethylamino)triphenylamine-functionalized aromatic polyamides, Macromolecules 41 (8) (2008) 2800–2808, https://doi.org/10.1021/ma702426z.
[47] N. Elgrishi, K.J. Rountree, B.D. McCarthy, E.S. Rountree, T.T. Eisenhart, J. L. Dempsey, A practical beginner's guide to cyclic voltammetry, J. Chem. Educ. 95 (2) (2018) 197–206, https://doi.org/10.1021/acs.jchemed.7b00361.
[48] M.E. Gomez, A.E. Kaifer, Voltammetric behavior of a ferrocene derivative: A comparison using surface-confined and diffusion-controlled species, J. Chem. Educ. 69 (6) (1992) 502, https://doi.org/10.1021/ed069p502.
[49] M.N. Ates, C.J. Allen, S. Mukerjee, K.M. Abraham, Electronic effects of substituents on redox shuttles for overcharge protection of Li-ion batteries, J. Electrochem. Soc. 159 (7) (2012) A1057, https://doi.org/10.1149/2.064207jes.
[50] J.A. Kowalski, M.D. Casselman, A.P. Kaur, J.D. Milshtein, C.F. Elliott, S. Modekrutti, N.H. Attanayake, N. Zhang, S.R. Parkin, C. Risko, F.R. Brushett, S. A. Odom, A stable two-electron-donating phenothiazine for application in nonaqueous redox flow batteries, J. Mater. Chem. A 5 (46) (2017) 24371–24379, 10.1039/C7TA05883G.
[51] H. Wang, S.Y. Sayed, E.J. Luber, B.C. Olsen, S.M. Shirurkar, S. Venkatakrishnan, U. M. Tefashe, A.K. Farquhar, E.S. Smotkin, R.L. McCreery, J.M. Buriak, Redox flow batteries: how to determine electrochemical kinetic parameters, ACS Nano 14 (3) (2020) 2575–2584, https://doi.org/10.1021/acsnano.0c01281.
[52] Y.R. In, J.M. Han, J.E. Kwon, B.G. Kim, H.C. Moon, Rational molecular design of electrochromic conjugated polymers: toward high-performance systems with ultrahigh coloration efficiency, Chem. Eng. J. 433 (2022) 133808, https://doi.org/10.1016/j.cej.2021.133808.
[53] R.S. Nicholson, Theory and application of cyclic voltammetry for measurement of electrode reaction kinetics, Anal. Chem. 37 (11) (1965) 1351–1355. 10.1021/ac60230a016.
[54] L. Wu, Y. Guo, G. Kuang, Y. Wang, H. Liu, Y. Kang, T. Ma, Y. Tao, K. Huang, S. Zhang, Synthesis and electrochromic properties of all donor polymers containing fused thienothiophene derivatives with high contrast and color efficiency, Polymer 261 (2022) 125404, 10.1016/j.polymer.2022.125404.
[55] H.C. Lu, S.Y. Kao, H.F. Yu, T.H. Chang, C.W. Kung, K.C. Ho, Achieving low-energy driven viologens-based electrochromic devices utilizing polymeric ionic liquids, ACS Appl. Mater. Interfaces 8 (44) (2016) 30351–30361, https://doi.org/10.1021/acsami.6b10152.
[56] B.C. Pan, W.H. Chen, T.M. Lee, G.S. Liou, Synthesis and characterization of novel electrochromic devices derived from redox-active polyamide–TiO2 hybrids, J. Mater. Chem. C 6 (45) (2018) 12422–12428, https://doi.org/10.1039/C8TC04469D.
[57] H.T. Lin, J.T. Wu, M.H. Chen, G.S. Liou, Novel electrochemical devices with high contrast ratios and simultaneous electrochromic and electrofluorochromic response capability behaviours, J. Mater. Chem. C 8 (36) (2020) 12656–12661, https://doi.org/10.1039/D0TC03008B.
[58] J.H. Wu, G.S. Liou, High-performance electrofluorochromic devices based on electrochromism and photoluminescence-active novel poly(4-cyanotriphenylamine), Adv. Funct. Mater. 24 (41) (2014) 6422–6429, https://doi.org/10.1002/adfm.201401608.
[59] G.A. Corrente, S. Cospito, A.L. Capodilupo, A. Beneduci, Mixed-valence compounds as a new route for electrochromic devices with high coloration efficiency in the whole vis-NIR region, Appl. Sci. 10 (23) (2020) 8372.
[60] B. Gélinas, D. Das, D. Rochefort, Air-stable, self-bleaching electrochromic device based on viologen- and ferrocene-containing triflimide redox ionic liquids, ACS Appl. Mater. Interfaces 9 (34) (2017) 28726–28736, https://doi.org/10.1021/acsami.7b04427.
[61] Y. Shi, G. Wang, Q. Chen, J. Zheng, C. Xu, Electrochromism and electrochromic devices of new extended viologen derivatives with various substituent benzene,

Sol. Energy Mater. Sol. Cells 208 (2020) 110413, https://doi.org/10.1016/j.solmat.2020.110413.

[62] S. Zhao, W. Huang, Z. Guan, B. Jin, D. Xiao, A novel bis(dihydroxypropyl) viologen-based all-in-one electrochromic device with high cycling stability and coloration efficiency, Electrochim. Acta 298 (2019) 533–540, https://doi.org/10.1016/j.electacta.2018.12.135.

[63] F. Sun, H. Zhang, J. Cai, F. Su, Y. Tian, Y.J. Liu, Selenophene, thiophene, and furan functionalized π-extended viologen derivatives for tunable all-in-one ECDs, Sol. Energy Mater. Sol. Cells 250 (2023) 112106, https://doi.org/10.1016/j.solmat.2022.112106.